
Robust Nonlinear Component Estimation with Tikhonov Regularization

Reuben Feinman
 New York University
 reuben.feinman@nyu.edu

Nikhil Parthasarathy
 New York University
 np1742@nyu.edu

Abstract

Learning reduced component representations of data using nonlinear transformations is a central problem in unsupervised learning with a rich history. Recently, a new family of algorithms based on maximum likelihood optimization with change of variables has demonstrated an impressive ability to model complex nonlinear data distributions. These algorithms learn to map from arbitrary random variables to independent components using invertible nonlinear function approximators. Despite the potential of this framework, the underlying optimization objective is ill-posed for a large class of variables, inhibiting accurate component estimates in many use cases. We present a new Tikhonov regularization technique for nonlinear independent component estimation that mediates the instability of the algorithm and facilitates robust component estimates. In addition, we provide a theoretically grounded procedure for feature extraction that produces PCA-like representations of nonlinear distributions using the learned model. We apply our technique to a handful of nonlinear data manifolds and show that the resulting representations possess important consistencies lacked by unregularized models.

1 Introduction

A fundamental problem of unsupervised learning is to uncover the nonlinear degrees of freedom that underlie observations from an unknown multidimensional data distribution. This task, known as nonlinear component analysis, amounts to finding a transformation f that maps the observed random variable to a new geometric space in which the dimensions of the data are independently distributed. Given observations of a random variable (r.v.) X with unknown distribution $p_X(x)$, the objective is to create an auxiliary r.v. $Y = f(X)$ such that $p_Y(y)$ has a simple, fully-factorized distribution.

The change of variables theorem of calculus dictates that, for an invertible function $f : \mathcal{R}^D \rightarrow \mathcal{R}^D$ that maps a r.v. X to a new r.v. $Y = f(X)$, the densities $p_X(x)$ and $p_Y(y)$ are related by the formula

$$p_X(x) = p_Y(f(x)) * |\det J_f(x)|, \quad (1)$$

where $J_f(x)$ is the Jacobian matrix of f evaluated at x . This relationship provides the inspiration for a new family of nonlinear component analysis techniques that has risen to prominence [4, 12, 5, 7]. These techniques capitalize on the capacity of neural networks to approximate complex functions. They propose to use gradient-based optimization to estimate the function f that maps an arbitrary r.v. X to a new r.v. Y with a target distribution that is fully-factorized. Given target distribution $p_Y(y)$, the approach is to specify an invertible, parameterized function f and to optimize this function such that the average log-likelihood of the observed data is maximized. For a dataset $\mathbf{X} = \{x_1, \dots, x_N\}$

containing N observations, the objective is written

$$\begin{aligned} f^* &= \arg \max_f \frac{1}{N} \sum_{n=1}^N \log p_X(x_n) \\ &= \arg \max_f \frac{1}{N} \sum_{n=1}^N \log p_Y(f(x_n)) + \log |\det J_f(x_n)|. \end{aligned} \quad (2)$$

This learning framework—henceforth denoted *nonlinear independent component estimation* (NICE), borrowing from Dinh et al. [4]¹—offers an optimization-based alternative to spectral dimensionality reduction techniques [14, 15, 13]. Like spectral techniques, NICE aims to estimate the independent components of nonlinear data manifolds. A key difference, however, is that NICE algorithms do not require the user to specify a target dimensionality *a priori*; the intrinsic dimensionality of the manifold is learned from the observations and allowed to vary as a function of the input. Furthermore, by harnessing high-capacity function approximators, NICE offers the capability to disentangle highly complex data distributions, such as the distribution of natural images. Spectral methods, which rely on Euclidean distances, have been largely unsuccessful with distributions of this kind.

Despite the great promise of NICE techniques, a major concern regarding the stability of these algorithms remains unaddressed. When the intrinsic dimensionality of the data is smaller than its apparent dimensionality, the NICE optimization objective becomes unstable. As we show in Section 4, accurate estimation of f^* in such case requires that some singular values of $J_f(x)$ approach infinity in neighborhoods of small intrinsic dimensionality. Consequently, models without proper regularization will struggle to produce accurate component estimates for many high-dimensional distributions. Progress in this area has been largely measured by the quality of generated samples, leaving a number of open questions about the consistencies of learned component representations.

The principal contribution of this work is a new regularization method for NICE, motivated by Tikhonov regularization from classical statistics, that stabilizes the optimization procedure. This method is agnostic to choice of architecture and requires little modification to the existing framework. In addition to this technique, we draw from fundamental component analysis and develop a new procedure for feature extraction that enables a practitioner to interpret and apply the learned representations of NICE models. We show that our regularized model produces robust component estimates in a handful of nonlinear data environments that are consistent with the underlying distribution. An unregularized version of our model, as well as the unmodified RealNVP [5] architecture, develops representations that lack these critical consistencies.

2 Related Work

Our work is closely tied to two families of literature from unsupervised learning: generative modeling of probability distributions and nonlinear dimensionality reduction.

Nonlinear dimensionality reduction by spectral decomposition is a well-studied field, an excellent overview of which is provided in Lawrence [10]. While spectral methods often perform well learning a fixed low-dimensional representation of high-dimensional data, they do not provide a density model of the observed variable; thus, these models cannot be used to draw samples or evaluate likelihoods. Furthermore, spectral techniques require the practitioner to specify a target dimensionality for the distribution in question, which can be problematic in situations of limited domain knowledge. Lastly, spectral techniques rely on distance metrics in Euclidean space, and these metrics perform poorly in domains such as natural images. In such domains, Euclidean distances are ineffective at capturing perceptually-relevant similarities between observations [9].

Generative modeling with deep nonlinear architectures has made many significant advances in recent years. The introduction of variational auto-encoders (VAEs) [8] has allowed for effective learning of an approximate posterior distribution through maximizing a variational lower bound on the log-likelihood of the data. A pitfall of VAEs, however, is their reliance on a reconstruction term in the objective as result of an imperfect decoder. The standard term is mean squared error in Euclidean

¹We use this term throughout the paper to refer to optimization-based component estimation with function approximators and change of variables, a more general class of algorithms than Dinh et al. [4].

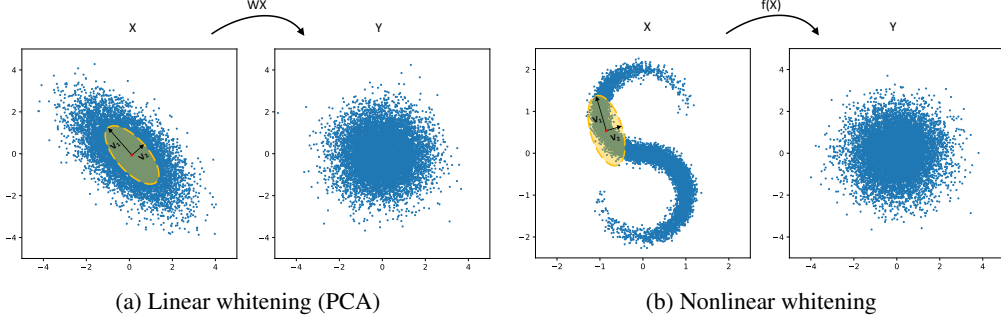


Figure 1: Linear and nonlinear whitening transformations. (a) A linear whitening transformation $Y = WX$ maps a Gaussian r.v. $X \sim \mathcal{N}(0, \Sigma_X)$ to isotropic Gaussian $Y \sim \mathcal{N}(0, I)$. The covariance estimate, $\hat{\Sigma}_X = (W^T W)^{-1}$, is fixed across the input space. (b) A nonlinear whitening transformation $Y = f(X)$ maps a non-Gaussian r.v. $X \sim p_X(x)$ to isotropic Gaussian $Y \sim \mathcal{N}(0, I)$. The local covariance estimate, $\hat{\Sigma}(x) = (J_f(x)^T J_f(x))^{-1}$, varies as a function of the input and is specified by the Jacobian matrix J_f . In both (a) and (b), blue dots show samples of the observed variable X (left) and of the transformed variable Y (right). Black vectors (left) convey the local component directions and magnitudes of p_X at a particular input location.

space, which, as explained, can be problematic for domains such as natural images. Furthermore, like spectral methods, VAEs force the specification of a desired dimensionality through the bottleneck layer size. This again limits the scope of these methods in settings where knowledge about the intrinsic dimensionality is limited. Generative Adversarial Networks (GANs) [6] are a related class of deep generative models that have successfully modelled complex nonlinear distributions. These algorithms learn to produce convincing samples of the data; however, they require careful hyperparameter tuning, the diversity of the generated samples is difficult to measure, and interpretation of the learned distribution is not well understood. Although both GANs and VAEs learn a mapping from independent components to complex distributions, neither has been carefully studied from the perspective of fundamental component analysis.

A separate class of deep generative models based on invertible nonlinear functions and the NICE objective of Eq. 2 offers some significant advantages over VAEs and GANs. First, by utilizing a "perfect decoder" [3], these methods avoid the concerns about Euclidean-based reconstruction terms that burden VAEs. Second, these algorithms offer the ability to learn the intrinsic dimensionality of the observed distribution from observations, which is beneficial in situations of limited domain knowledge. Although this framework was only formally developed in recent years [4, 12, 5], the change-of-variables formula for learning invertible transformations of probability distributions has appeared in other contexts, such as the maximum likelihood formulation of ICA [2] and efforts to Gaussianize natural images [1]. More recently, an updated architecture and algorithm known as RealNVP [5] (Appendix B.2) has demonstrated an impressive ability to model complex distributions. In this paper, we discuss the optimization objective used by models of the NICE class. We connect this framework to fundamental component analysis and propose a new regularization technique to help avoid overfitting and facilitate robust component estimates.

3 Nonlinear Independent Component Estimation (NICE)

We begin with a rigorous theoretical analysis of the NICE objective. Throughout the section, assume we are given a dataset $\mathbf{X} = \{x_1, \dots, x_N\}$ with N observations of an r.v. $X \in \mathcal{R}^D$, and that the dataset has been centered such that each dimension has zero mean. Furthermore, assume that we'd like to learn an invertible mapping $f : \mathcal{R}^D \rightarrow \mathcal{R}^D$ such that $Y = f(X)$ is distributed according to a simple isotropic Gaussian, i.e. $p_Y(y) = \mathcal{N}(y; 0, I)$. In Section 5, we show that distributions with non-Gaussian latent structure can be well-modeled using Gaussian targets and deep architectures.

3.1 Linear component estimation (PCA)

If we restrict our functional mapping f to be linear, e.g. $f(X) = WX$ for some matrix $W \in \mathcal{R}^{D \times D}$, then the NICE objective of Eq. 2 reconstructs Principal Component Analysis (PCA). In the case of

linear f , the objective is written as

$$W^* = \arg \max_W \frac{1}{N} \sum_{n=1}^N \log p_Y(Wx_n) + \log |\det W|.$$

Noting that $\log p_Y(Wx_n) = -\frac{1}{2}\|Wx_n\|_2^2 + \text{const.}$, and that $\log |\det W| = \frac{1}{2}\log\det(W^T W)$, this objective becomes

$$\begin{aligned} W^* &= \arg \max_W \frac{1}{N} \sum_{n=1}^N -\frac{1}{2}\|Wx_n\|_2^2 + \frac{1}{2}\log\det(W^T W) \\ &= \arg \min_W \frac{1}{N} \sum_{n=1}^N \|Wx_n\|_2^2 - \log\det(W^T W). \end{aligned} \quad (3)$$

Some algebra shows that this objective is equivalent to maximum likelihood estimation of $p_X(x)$ under the assumption that the distribution is Gaussian, i.e. that $p_X(x) = \mathcal{N}(x; 0, \Sigma)$. The average log-likelihood of observation set \mathbf{X} given parameter Σ is written as

$$L(\Sigma; \mathbf{X}) = \frac{1}{N} \sum_{n=1}^N -\frac{1}{2}x_n^T \Sigma^{-1} x_n - \frac{1}{2}\log\det(\Sigma) - \frac{D}{2}\log(2\pi).$$

A Gaussian precision matrix is positive semi-definite; therefore, we can write our precision estimate as $\hat{\Sigma}^{-1} = W^T W$ for square matrix W , and the MLE objective becomes

$$\begin{aligned} W^* &= \arg \min_W \frac{1}{N} \sum_{n=1}^N \frac{1}{2}x_n^T W^T W x_n + \frac{1}{2}\log\det((W^T W)^{-1}) \\ &= \arg \min_W \frac{1}{N} \sum_{n=1}^N \|Wx_n\|_2^2 - \log\det(W^T W), \end{aligned} \quad (4)$$

reproducing the NICE objective of Eq. 3. Given solution W^* , the singular value decomposition (s.v.d.) $W^* = USV^T$ yields an orthogonal matrix V whose column vectors v_i are the principal components of the data and a diagonal matrix S whose squared diagonal entries s_i^2 are the corresponding precision values (inverse variances).²

3.2 Nonlinear component estimation

Nonlinear component estimation is an extension of the linear case that handles situations where the data distribution $p_X(x)$ is non-Gaussian. For such a distribution, the mapping $Y = f(X)$ must be nonlinear in order to obtain isotropic Gaussian components $Y \sim \mathcal{N}(0, I)$.

For an isotropic Gaussian target distribution, the generalized NICE objective of Eq. 2 is written as

$$f^* = \arg \min_f \frac{1}{N} \sum_{n=1}^N \|f(x_n)\|_2^2 - \log\det(J_f(x_n)^T J_f(x_n)), \quad (5)$$

where $J_f(x_n)$ is the Jacobian matrix of f evaluated at x_n . Comparing to the Gaussian MLE objective of Eq. 4, note that the precision estimate $\hat{\Sigma}^{-1} = W^T W$ has been replaced by an estimate $\hat{\Sigma}^{-1}(x) = J_f(x)^T J_f(x)$ that varies as a function of x . The second term of the objective's summation, which can be brought outside of the sum in Eq. 4 if scaled by a constant, must now remain inside the sum, for it depends on x_n .

The connection to PCA provides key insights about the nonlinear case. Whereas PCA produces a linear whitening transformation for Gaussian data, NICE produces a *nonlinear whitening transformation* that maps a non-Gaussian variable X to isotropic Gaussian. As visualized in Fig. 1, this nonlinear transformation bears information about the local covariance of X at each region of the input space. Given the solution f^* that maps X to isotropic Gaussian, the local component directions and variances of the data manifold at each input point are specified by the s.v.d. of the Jacobian matrix, $J_f(x) = USV^T$: the orthogonal matrix V holds the directions in its column vectors, and the diagonal matrix S holds the corresponding inverse standard deviations in its diagonal entries ($\lambda_i = s_i^{-2}$ gives the variance for the i -th component).

²The precision estimate is written $\hat{\Sigma}^{-1} = W^T W = (USV^T)^T USV^T = VS^T U^T USV^T = VS^2 V^T$.

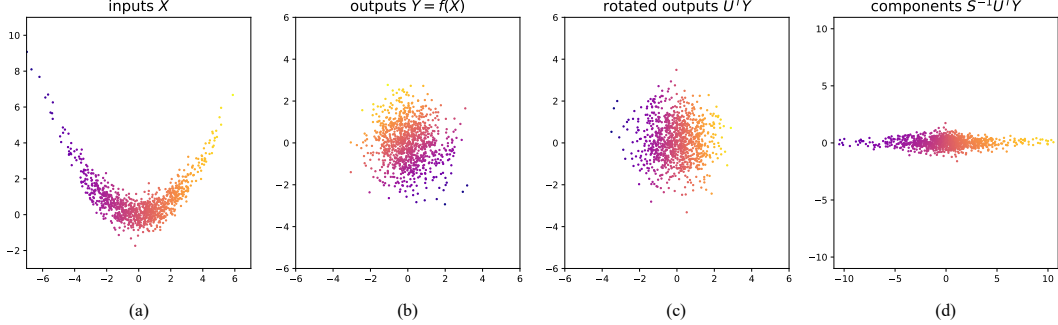


Figure 2: Computing component representations for nonlinear distributions using a function f that maps to isotropic Gaussian. (a) Samples from a 2D nonlinear banana distribution. (b) Transformed samples output by a function $Y = f(X)$ that maps the original distribution to a standard normal. (c) Each output is rotated by a unique orthogonal matrix U determined from the Jacobian s.v.d. at the corresponding input ($J_f(x) = USV^T$). (d) Each rotated output is next scaled by a unique diagonal matrix S^{-1} determined from the Jacobian s.v.d.

3.3 Computing nonlinear component projections

PCA yields a linear basis that serves as a powerful feature representation for Gaussian-like variables. Nonlinear component estimation provides a useful analogue to PCA for non-Gaussian data; however, applications of NICE have focused primarily on sampling and density estimation. In some cases, whitened components $Y = f(X)$ are applied as a feature representation for tasks such as manifold traversal and classification [5, 11]. This feature space is problematic, however, because insignificant components have been expanded to unit variance. Here, we describe a simple procedure to extract unwhitened component representations from NICE-optimized functions.

Given a non-Gaussian r.v. X and a function f that maps the variable to isotropic Gaussian, the Jacobian J_f can be used to uncover the component projection of each input point. The algorithm consists of inverting the whitening process of f at each output $y_n = f(x_n)$ using the s.v.d. of $J_f(x_n)$. Assuming the Jacobian at x_n factors as $J_f(x_n) = USV^T$, the component projection \hat{y}_n for the point is obtained by transforming the function output by the formula $\hat{y}_n = S^{-1}U^T y_n$. The first transformation, U^T , rotates each y_n such that its dimensions correspond to component axes. This step is necessary due to the non-uniqueness of f : there may be multiple functions that map the variable X to an isotropic Gaussian. The second transformation, S^{-1} , scales the components according to their standard deviations, giving emphasis to the components of greatest significance. To ensure consistent output from s.v.d., the columns of U are adjusted such that the loadings with largest magnitude are always positive.

As a demonstration, consider a r.v. $X \in \mathcal{R}^2$ drawn from a banana-shaped distribution, samples of which are shown in Fig. 2a. The variable is defined as $X = [2\epsilon_1, -4\epsilon_1^2/5 + \epsilon_2/2]$, with $\epsilon_i \sim \mathcal{N}(0, 1)$. Furthermore, consider the function $f(X) = [-X_1/4 - \sqrt{3}X_2 + \sqrt{3}X_1^2/5, \sqrt{3}X_1/4 - X_2 + X_1^2/5]$, one of many transformations that map X to $\mathcal{N}(0, I_2)$. Samples of the transformed variable $Y = f(X)$ are shown in Fig. 2b. The Jacobian J_f of this transformation is defined as

$$\begin{bmatrix} \partial f_1 / \partial X_1 & \partial f_1 / \partial X_2 \\ \partial f_2 / \partial X_1 & \partial f_2 / \partial X_2 \end{bmatrix} = \begin{bmatrix} -1/4 + 2\sqrt{3}X_1/5 & -\sqrt{3} \\ \sqrt{3}/4 + 2X_1/5 & -1 \end{bmatrix}$$

and varies as a function of the input. Computing the s.v.d $J_f(x) = USV^T$ for each point, we first use the left Jacobian singular matrix to rotate each output $y = U^T y$ (Fig. 2c). Next, we use the inverse singular value matrix of each point to scale the dimensions $y = S^{-1}y$ (Fig. 2d). The result is a factorized distribution whose dimensions correspond to the nonlinear components of the data and are scaled according to component variance.

4 Tikhonov Regularization

When the intrinsic dimensionality of the data is less than the apparent dimensionality, the NICE optimization algorithm becomes unstable. As a simple linear demonstration, consider a 1D Gaussian

that is embedded in a 2D space, specified by $p_X(x) = N(x; 0, \Sigma)$. The covariance matrix factors as $\Sigma = V\Lambda V^T$, where Λ is a diagonal matrix with diagonal entries $[\lambda_1, 0]$. The NICE algorithm, which is agnostic to the intrinsic dimensionality of the data a priori, attempts to learn a linear mapping $Y = WX$, with $W \in \mathcal{R}^{2 \times 2}$, that maps X to an isotropic Gaussian r.v. $Y \sim N(0, I_2)$. Given an observation set \mathbf{X} , the mapping matrix W is initialized at random with initial singular values $[s_1, s_2]$. Recall from Section 3.1 that the optimal mapping W^* has the following property: the inverse squared singular values s_i^{-2} correspond to the eigenvalues of the MLE covariance estimate. This covariance estimate is singular; therefore, the optimizer must push one of its singular values to infinity to reach the correct solution.

In classical statistics, a common technique to mediate singular covariances is to add a small value, α , to the diagonal entries of the empirical covariance S , such that $S' = S + \alpha I$. This technique, known as Tikhonov regularization (or *shrinkage*), provides additional robustness to statistical estimators at the cost of a small, often negligible estimation error. To understand the affect of this modification on Gaussian MLE, consider again the MLE objective of Eq. 4. Given empirical covariance $S = \frac{1}{N} \sum_{n=1}^N x_n x_n^T$, the objective can be re-written as

$$W^* = \arg \min_W \text{tr}(SW^T W) - \log \det(W^T W).$$

Adding a diagonal to the empirical covariance, this objective becomes

$$\begin{aligned} W^* &= \arg \min_W \text{tr}((S + \alpha I)W^T W) - \log \det(W^T W) \\ &= \arg \min_W \text{tr}(SW^T W) - \log \det(W^T W) + \alpha * \|W\|_F^2. \end{aligned}$$

Thus, Tikhonov regularization is implemented by simply adding an L2 penalty on W to our optimization objective, with penalty weight α . In the linear case, the Jacobian of the function f that maps X to an isotropic Gaussian is specified by the matrix W and is independent of the input. In general, however, the Jacobian matrix $J_f(x)$ is a function of x . Generalizing Tikhonov regularization to nonlinear component estimation, we place an L2 penalty on the Jacobian evaluated at each input. The objective of Eq. 5 then becomes

$$f^* = \arg \min_f \frac{1}{N} \sum_{n=1}^N \|f(x_n)\|_2^2 - \log \det(J_f(x_n)^T J_f(x_n)) + \alpha * \|J_f(x_n)\|_F^2. \quad (6)$$

Thus, applying Tikhonov regularization to NICE is as simple as placing an L2 penalty on the Jacobian matrix $J_f(x_n)$ at each data point x_n . This regularization term stabilizes the algorithm and facilitates accurate nonlinear component estimation with black-box optimization (see Appendix A for demo).

5 Experiments

We evaluated the ability of Tikhonov-regularized nonlinear architectures to produce consistent component estimates from a handful of datasets, focusing on distributions with reduced intrinsic dimensionality. Each model was compared against an unregularized model of the same family. To keep our approach as general as possible, we applied generalized neural network architectures with minimal restriction (Appendix B). For an input variable with D dimensions, we constructed a multilayer feed-forward network composed of L hidden layers, each consisting of an $\mathcal{R}^D \rightarrow \mathcal{R}^D$ affine transformation coupled with an invertible, element-wise nonlinearity. An output layer with linear activation was appended to the end of the network. For each dataset and architecture, the network was initialized at random and trained via stochastic gradient descent with a batch size of 200 and the Adam optimizer. We used an isotropic Gaussian target distribution $p_Y(y) = \mathcal{N}(y; 0, I)$, with $Y \in \mathcal{R}^D$. Training data were centered such that each feature has zero mean. The experiments described here can be replicated using the provided code (Appendix C).

5.1 Nonlinear manifold learning

We started with two manifold learning tasks motivated by nonlinear dimensionality reduction literature [16], shown in in Fig 3. Each dataset consisted of 10,000 observations from a 2D latent distribution

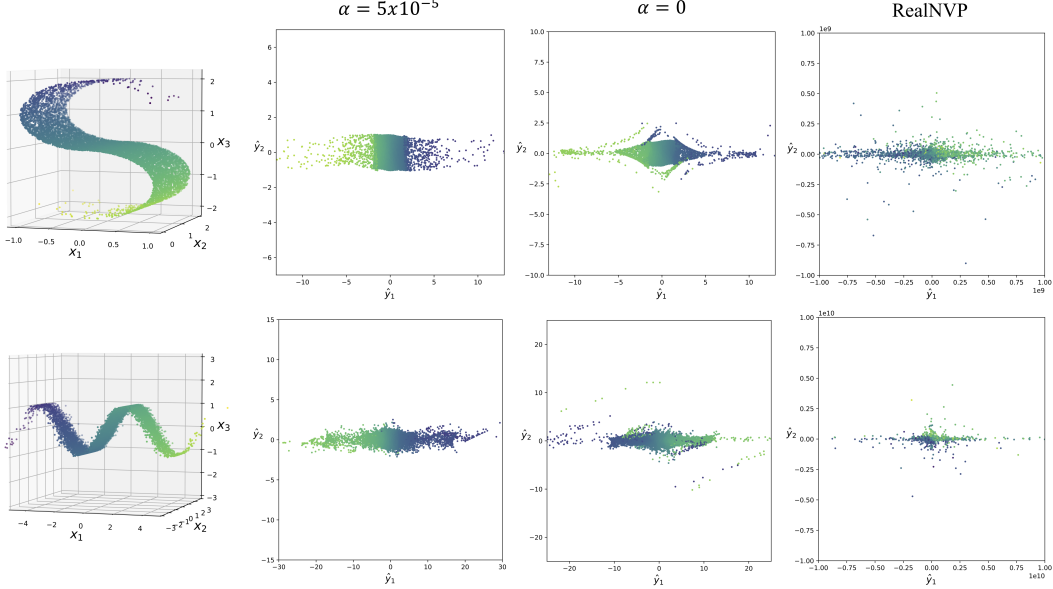


Figure 3: Results of NICE models applied to two nonlinear manifolds. The source distributions (left) are 2D manifolds embedded in a 3D space (top row: “S-curve” dataset, bottom row: sine wave dataset). Plots show the nonlinear component projections of the data computed with each model after training. Our regularized model ($\alpha = 5 \times 10^{-5}$) successfully estimates the nonlinear components. Neither an unregularized version of our model ($\alpha = 0$) or an unmodified RealNVP architecture produce consistent component projections.

that has been embedded in a 3D space by a nonlinear transformation. The first dataset is a version of the synthetic “S-curve” manifold with one of two latent factors distributed as Gaussian. The second dataset consists of a sine wave with 2D Gaussian latent structure ($X = [2\epsilon_1, \epsilon_2/2, \sin(2\epsilon_1)]$, $\epsilon_i \sim \mathcal{N}(0, 1)$). For each of these datasets, we applied a multilayer architecture with 8 hidden layers and the inverse hyperbolic sine nonlinearity. This nonlinearity has the nice property of a smooth gradient and both a domain and range of \mathcal{R} . With Tikhonov regularization applied ($\alpha = 5 \times 10^{-5}$), we found that the network learns a strong estimate of the underlying 2D latent structure in both cases. Plots show the projections \hat{Y} of each point onto the top 2 components of the learned model, obtained using the algorithm from Section 3.3. Interestingly, the network is able to uncover non-Gaussian latent structure from the S-curve dataset using Gaussian component targets. Without regularization, the network fails to produce a coherent estimate of the underlying latent structure in either case.

We further tested the RealNVP architecture (Appendix B.2) on these same two nonlinear distributions, again using Adam with a batch size of 200. RealNVP is an invertible feed-forward architecture composed of simple coupling layers with triangular Jacobian, lending to cheap likelihood computation. We used a model with 6 coupling layers, each composed of log-scale and shift functions parameterized by neural networks with 2 hidden layers of 512 ReLU units (default parameters of the TensorFlow RealNVP implementation), and a masking dimensionality $d = 1$. Following standard practices, the dimensions are permuted after each layer and batch normalization is applied to improve training performance. Interestingly, the network’s training loss converges without Jacobian regularization, and samples from the model are visually consistent with samples from both our regularized model and ground truth. However, component projections extracted from this architecture lack coherent structure and are many orders of magnitude larger than those of the standard network.

5.2 Learning MNIST digits

Our 3D manifold learning tasks demonstrate the importance of regularization to producing accurate estimates of nonlinear independent components. We next set out to test the effect of Tikhonov regularization on likelihood generalization and sample quality. A primary question of ours is whether the quality of generated samples alone is sufficient proof of a rich internal model. The MNIST handwritten digits dataset provides a setting of increased complexity over our 3D distributions where samples are easy to visualize and interpret.

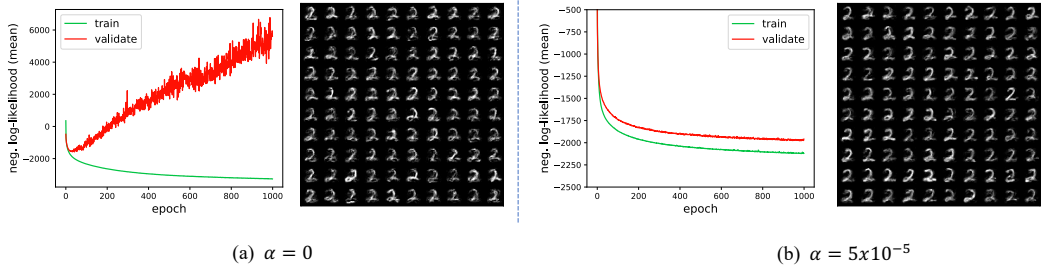


Figure 4: Regularized vs. unregularized component estimation applied to 28x28 images of MNIST 2's. (a) With no regularization, the model overfits severely to the training data. (b) With regularization applied, the model exhibits strong generalization performance. Samples from the resulting model are shown next to each plot.

We applied our component estimation algorithm to the MNIST image dataset, comparing a regularized model against its unregularized counterpart. The dataset consists of 28x28 images with values in range [0,1]. We trained our model on the manifold of image class “2”, providing 5958 points for training and 1032 points for validation. Images were flattened to dimensionality 784, and we applied an architecture from the family discussed above with 6 hidden layers and inverse hyperbolic sine nonlinearity. Learning trajectories on the train and validation sets, as well as samples from the resulting model, are shown for an unregularized architecture ($\alpha = 0$) in Fig. 4a. In 4b, analogous results are shown for a regularized model ($\alpha = 5 \times 10^{-5}$) with all other hyperparameters equivalent. It can be seen that the unregularized MNIST model exhibits significant over-fitting during the course of training, achieving average log-likelihoods of 3,265 and -5,659 on the training and validation sets, respectively. The Tikhonov-regularized model, however, exhibits strong generalization performance, achieving train and validation scores of 2,111 and 2,014. The regularized model has notably better sample quality overall, characterized by less noise in many of the images. Interestingly, samples generated by the unregularized model share many consistencies with ground truth, in spite of poor generalization performance on the log-likelihood task. This result suggests that sample quality alone may provide insufficient proof of a rich generative model. One possible explanation is that the unregularized model learns to memorize the training data, whereas the regularized model learns a generalizable feature representation. Further experiments are necessary to validate this hypothesis.

As an additional evaluation, we tested our regularized model’s ability to produce coherent low-dimensional component representations of the MNIST image data. We selected 1,000 images at random from the training set and used our component projection algorithm to extract the top 2 components of the model for each image. The 2D points for each image are plotted in Fig. 5. The model produces a qualitatively meaningful representation of the image manifold wherein 2’s of similar drawing style are grouped together, capturing a combination of properties such as digit angle, line thickness, and curved vs. straight lines.

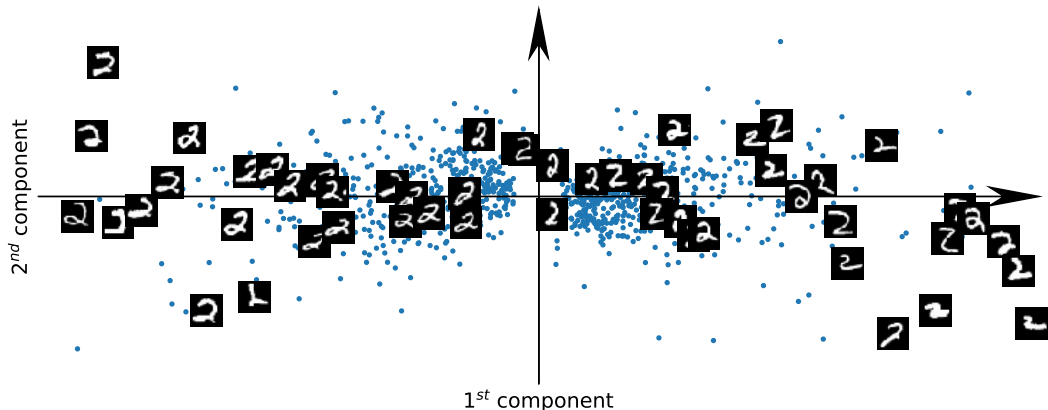


Figure 5: Top 2 component projections for MNIST 2's. Projections for 1,000 training images are obtained from the regularized MNIST model ($\alpha = 5 \times 10^{-5}$) using the algorithm of Section 3.3.

6 Discussion

In this work, we develop a more robust and interpretable framework for nonlinear independent component estimation. We leverage recent work to show that a Tikhonov-regularized version of the NICE estimation procedure can address significant instability issues when the intrinsic dimensionality of the input data is smaller than the total number of input features. In addition, while previous work in this space has focused on sampling and density estimation with NICE-optimized representations, we develop a component extraction method that allows for new interpretation of the specific basis features in a manner analogous to linear methods such as PCA. In future work, we hope to test our methodology on higher dimensional natural image datasets and compare the learned component representations to the features developed by other deep generative models. In addition, we'd like to apply our feature extraction method to analyze and understand the representations of other algorithms that learn a mapping between isotropic Gaussians and complex distributions. This includes (but is not limited to) the generator network of a GAN and the decoder of a VAE.

References

- [1] Johannes Ballé, Valero Laparra, and Eero P. Simoncelli. Density modeling of images using a generalized normalization transformation. In *ICLR*, 2016.
- [2] Anthony J Bell and Terrence J Sejnowski. An information-maximization approach to blind separation and blind deconvolution. *Neural computation*, 7(6):1129–1159, 1995.
- [3] Yoshua Bengio. How auto-encoders could provide credit assignment in deep networks via target propagation. *arXiv preprint arXiv:1407.7906*, 2014.
- [4] Laurent Dinh, David Krueger, and Yoshua Bengio. NICE: Non-linear independent components estimation. In *ICLR*, 2015.
- [5] Laurent Dinh, Jascha Sohl-Dickstein, and Samy Bengio. Density estimation using Real NVP. In *ICLR*, 2017.
- [6] Ian Goodfellow, Jean Pouget-Abadie, Mehdi Mirza, and et al. Generative adversarial nets. In *NIPS*, 2014.
- [7] Diederik P. Kingma and Prafulla Dhariwal. Glow: Generative flow with invertible 1x1 convolutions. In *NIPS*, 2018.
- [8] Diederik P. Kingma and Max Welling. Auto-encoding variational bayes. In *ICLR*, 2013.
- [9] Valero Laparra, Johannes Ballé, Alexander Berardino, and Eero P Simoncelli. Perceptual image quality assessment using a normalized laplacian pyramid. *Electronic Imaging*, 2016(16):1–6, 2016.
- [10] Neil Lawrence. A unifying probabilistic perspective for spectral dimensionality reduction: Insights and new models. *Journal of Machine Learning Research*, 13:1609–1638, 2012.
- [11] Eric Nalisnick, Akihiro Matsukawa, Yee Whye Teh, Dilan Gorur, and Balaji Lakshminarayanan. Hybrid models with deep and invertible features. In *ICML*, 2019.
- [12] Danilo Jimenez Rezende and Shakir Mohamed. Variational inference with normalizing flows. In *ICML*, 2015.
- [13] Sam T Roweis and Lawrence K Saul. Nonlinear dimensionality reduction by locally linear embedding. *Science*, 290(550):2323–2326, 2000.
- [14] Bernhard Scholkopf, Alexander Smola, and Klaus-Robert Muller. Nonlinear component analysis as a kernel eigenvalue problem. *Neural Computation*, 10:1299–1319, 1998.
- [15] Joshua B Tenenbaum, Vin De Silva, and John C Langford. A global geometric framework for nonlinear dimensionality reduction. *Science*, 290(550):2319–2323, 2000.
- [16] Xianglei Xing, Sidan Du, and Kejun Wang. Robust hessian locally linear embedding techniques for high-dimensional data. *Algorithms*, 9(36):36, 2016.

A Tikhonov Regularization Stabilizes NICE

Fig. 6 shows a demonstration of the affect of Tikhonov regularization in two simple component estimation use cases, one linear and another nonlinear. In each case, the observed variable has an intrinsic dimensionality that is smaller than the number of inputs. The optimal mapping f is determined by gradient-based optimization. For the linear case, the mapping is specified by $Y = WX$, where W is a weight matrix that is learned during optimization. For the nonlinear case, the function is specified as $Y = f(X)$, where f is parameterized by a simple invertible neural network model whose parameters are learned during optimization. In each case, without regularization the optimization algorithm fails to converge to the correct solution. When Tikhonov regularization is added to the objective, the algorithm successfully converges to the correct solution.

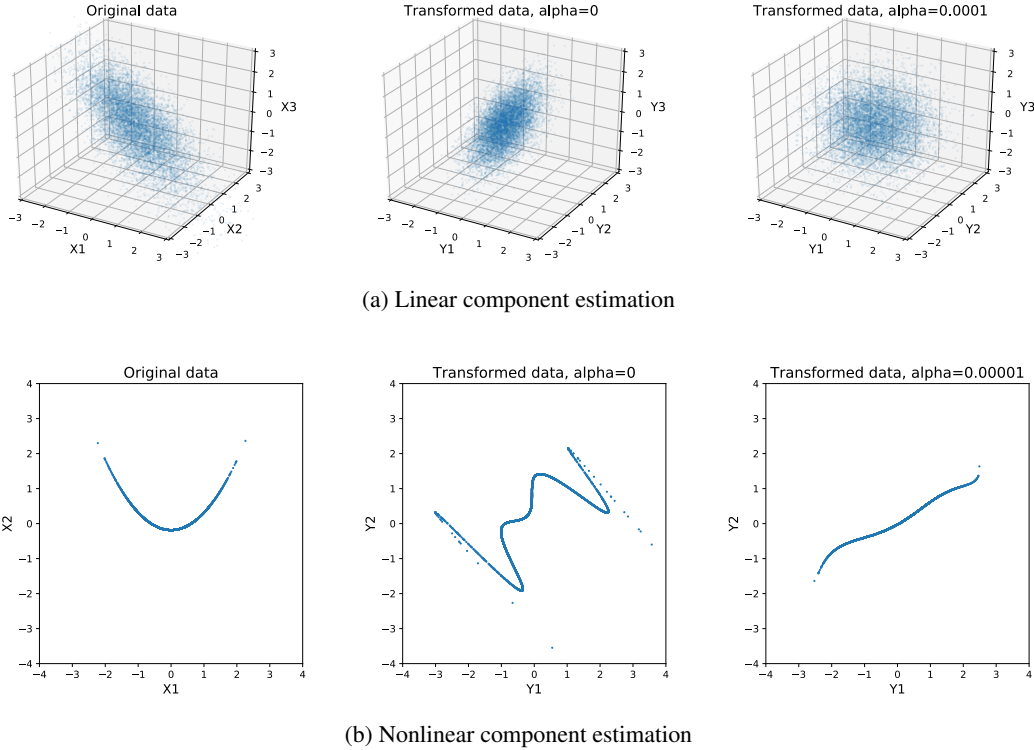


Figure 6: Tikhonov regularization stabilizes optimization-based component estimation. (a) Linear component estimation was performed on observations from a 2D Gaussian embedded in a 3D space. The original centered dataset is shown (left). The transformation $Y = WX$ was initialized at random and optimized via gradient descent. Without Tikhonov regularization, the algorithm fails to converge to the correct components (middle). With regularization weight $\alpha = 10^{-4}$, the algorithm converges to the correct data components (right). (b) Nonlinear component estimation was performed on observations from a 1D nonlinear data manifold embedded in a 2D space. The original centered dataset is shown (left). The function estimator $Y = f(X)$ is parameterized by a neural network with 6 hidden layers of 2 units, each with softplus nonlinearity, and a final linear layer with 2 units. The network parameters are initialized at random and optimized via gradient descent. Without Tikhonov regularization, the algorithm fails to converge to the correct components (middle). With regularization weight $\alpha = 10^{-5}$, the algorithm converges to the correct data components (right).

B Generalized Invertible Function Approximators

In our experiments, we use a generalized deep neural network architecture to parameterize the NICE invertible function approximator. This contrasts with recent works from the NICE literature that have used restricted architectures to make Jacobian determinant computations more tractable (see B.1 and B.2). Our experiments are designed to isolate the affect of Tikhonov regularization on the NICE objective. Although our algorithm is agnostic to choice of architecture, and therefore can be applied to restricted models, we use a generalized architecture in our experiments and sideline concerns about

training speed. For an observed variable $X \in \mathcal{R}^D$, our neural network is composed by stacking L standard layers, each with an affine transformation followed by an element-wise non-linearity. Each transformation is $f : \mathcal{R}^D \rightarrow \mathcal{R}^D$.

Here, we briefly review a few restricted architectures from the NICE literature.

B.1 Normalizing flows

Normalizing flows are specialized architectures composed of nonlinear transformations called *flow layers* [12]. These layers are designed to exploit various determinant identities, such as the Matrix Determinant Lemma, and facilitate fast Jacobian determinant computation. The original paper proposed two types of flow layers: *planar flows* and *radial flows*.

B.2 RealNVP

RealNVP [5] is a specialized architecture composed of partitioned nonlinear transformations called *coupling layers*. Coupling layers are designed to have triangular Jacobian, making Jacobian determinant computation very fast. For each layer, the user specifies a partitioning dimensionality d , and the transformation that maps inputs $X \in \mathcal{R}^D$ to outputs $Y \in \mathcal{R}^D$ is defined as

$$\begin{aligned} Y_{1:d} &= X_{1:d} \\ Y_{d+1:D} &= X_{d+1:D} \odot \exp(s(X_{1:d})) + t(X_{1:d}), \end{aligned} \tag{7}$$

where s and t are the log-scale and shift functions, respectively. RealNVP is an extension of an earlier model that used coupling layers without a log-scale function [4].

C Code

All experiments from this paper can be replicated using the source code repository located at <http://github.com/rfeinman/manifold-learning>. Instructions for running the experiments are provided in the repository Readme.